BREAKTHROUGHS IN LOW-PROFILE LEAKY-WAVE HPM ANTENNAS

Prepared by: Robert A. Koslover

Scientific Applications & Research Associates, Inc.
6300 Gateway Drive
Cypress, CA 90630-4844

18 June 2014

Data Item: A001 - Progress, Status, & Management Quarterly Report #3

Prepared for:

Program Officer: Lee Mastroianni
ONR Code 30

OFFICE OF NAVAL RESEARCH
875 North Randolph Street
Suite 1425
Arlington, VA 22203-1995

REPORT DOCUMENTATION PAGE

Form Approved
OMB No. 0704-0188

1. REPORT DATE *(DD-MM-YYYY)*	**2. REPORT TYPE**	**3. DATES COVERED** *(From - To)*
18-06-2014	Quarterly	13 Mar 2014 – 18 Jun 2014

4. TITLE AND SUBTITLE
Breakthroughs in Low-Profile Leaky-Wave HPM Antennas
Progress, Status, & Management Report
(Quarterly Report #3)

5a. CONTRACT NUMBER
N00014-13-C-0352

5b. GRANT NUMBER

5c. PROGRAM ELEMENT NUMBER

6. AUTHOR(S)
Koslover, Robert, A.

5d. PROJECT NUMBER

5e. TASK NUMBER

5f. WORK UNIT NUMBER

7. PERFORMING ORGANIZATION NAME(S) AND ADDRESS(ES)

Scientific Applications &
Research Associates, Inc.
6300 Gateway Drive
Cypress, CA 90630-4844

8. PERFORMING ORGANIZATION REPORT NUMBER

9. SPONSORING / MONITORING AGENCY NAME(S) AND ADDRESS(ES)
Office of Naval Research
875 North Randolph Street
Suite 1425
Arlington, VA 22203-1995

10. SPONSOR/MONITOR'S ACRONYM(S)
Code 30

11. SPONSOR/MONITOR'S REPORT NUMBER(S)

12. DISTRIBUTION / AVAILABILITY STATEMENT
Distribution Statement A. Approved for public release; distribution is unlimited.

13. SUPPLEMENTARY NOTES
..

14. ABSTRACT
This report describes progress during the 3rd quarter of this program and summarizes the current status of the research. Our primary technical activities this period consisted of investigating the effects of mutual coupling between leaky-wave channels and extending / improving our evolving toolset for the design of HPM-capable forward-traveling leaky-wave antennas.

15. SUBJECT TERMS
Leaky-wave Antennas. High Power Microwaves (HPM) Antennas. Low-profile Conformal Antennas.

16. SECURITY CLASSIFICATION OF:			**17. LIMITATION OF ABSTRACT**	**18. NUMBER OF PAGES**	**19a. NAME OF RESPONSIBLE PERSON (Monitor)**
a. REPORT	**b. ABSTRACT**	**c. THIS PAGE**			Lee Mastroianni
Unclassified	Unclassified	Unclassified	SAR	___	**19b. TELEPHONE NUMBER**(incl. area code) (703) 696-3073

Standard Form 298 (Rev. 8-98)
Prescribed by ANSI Std. Z39.18

Table of Contents

List of Figures

1. INTRODUCTION

This is SARA's *3rd* Quarterly Report for "Breakthroughs in Low-profile Leaky-Wave HPM Antennas," a 37-month Basic Research effort, sponsored by the US Office of Naval Research (ONR). This work includes fundamental theoretical analyses, numerical modeling, and related basic research. Objectives include to discover, identify, investigate, characterize, quantify, and document the performance, behavior, and design of innovative High Power Microwave (HPM, GW-class) antennas of the *forward-traveling, fast-wave, leaky-wave* class.

1.1. Overview of Previous Activities (1st and 2nd Quarter)

During the *first* quarter, we prepared and established useful equations and algorithms for predicting reflections and transmission of incident TE waves from parallel-wire grills, dielectric windows, and combinations of wire grills with dielectric windows, in problems reducible to purely H-plane (2D) representations. We then applied this theory to guide the design of high-gain configurations (again, limited to 2D, H-plane representations) for linear, forward traveling-wave, leaky-wave antennas. The theory built upon equivalent circuit methods and wave matrix theory, which provided useful formalisms upon which we continue to build.

During the *second* quarter, we pursued initial extensions of the previous work into three dimensions, in order to include phenomena with E-plane dependencies. We succeeded in adding into the wave-matrix formalism the reflection/transmission properties associated with the transition to free space from a *finite-width* leaky-wave channel, including the edge-tapering essential to HPM applications. These geometric aspects do not arise in analyses confined to the H-plane alone. As expected, our 3D analyses were somewhat more reliant on numerical models than in the 2D analyses, due to the greater complexity of identifying and/or building practical analytic approaches capable of addressing true 3D geometries of interest. For more information, we refer the reader to our *Quarterly Report #1* and *Quarterly Report #2*.

1.2. Overview of Recent Activities (3rd Quarter)

During the *third* quarter, we pursued a variety of continuing and new analyses/design activities, many of which are still in-progress. One emphasis during this period was exploration of channel-to-channel coupling (aka, mutual coupling) which (as we have noted earlier) is an important design concern, since it can impact antenna performance significantly in terms of gain, peak power-handling, and impedance matching. Our approach here leverages mostly numerical methods, but with intuitive considerations.

This report also includes a pleasingly-simple derivation (in 2D geometry) of an equation that tells how to position the leaky-grill relative to the opposite wall to compensate for changes in the phase velocity due to leakage through the grill. In the form derived, the result appears to be generalizable to 3D geometries.

In addition to those topics, we discuss some of the aperture geometries (shapes and curvatures) currently being investigated. Section 3 describes the technical work performed this quarter in more detail.

2. STATUS OF THE PLAN/SCHEDULE AND FUNDING

Figure 1 below maps out the overall program plan, for quick reference. As of the time of this report, we are continuing Tasks 2.1, 2.2, 3.1, and are initiating Tasks 2.3 and 3.2. The latter have been somewhat delayed relative to our initial plans, but we plan/expect to catch up over the next quarter.

The subject contract was awarded on 9/18/2013 and has an end date of 10/17/2016. The total contract value is $868,350, with current (per P00003 signed on 4/24/2014) allotted funding of $406,530. According to SARA's accounting system as of June 13, 2014, expenses (including fee) have totaled $211,116, thus leaving $195,414 remaining.

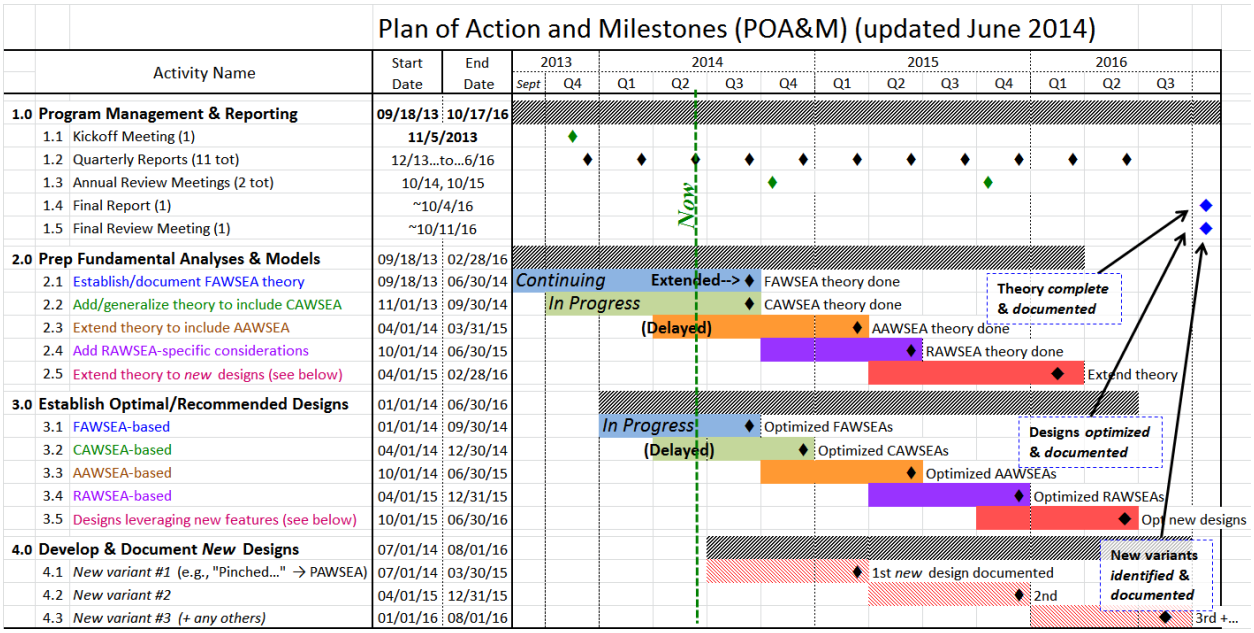

Figure 1. Overall program plan

3. RESEARCH PERFORMED THIS PERIOD

3.1. Investigations of Mutual Coupling

It would, of course, be very helpful if the design of forward-traveling leaky-wave HPM-capable antennas could proceed without consideration of the effects of mutual coupling between channels. However, such effects can and do have significant impact on resulting performance, leading to increased design time, uncertainty, and constraints on design choices. Mutual coupling has long received attention[1] in the literature, but the subject remains theoretically challenging, although simple parallel dipole elements have been analyzed theoretically in much detail[1]. The papers by S. Nishida[2] are perhaps the most relevant to our own work, but do not include essential geometric features (such as rounded edges, and not to even mention dielectric windows) required for HPM-capable designs.

In analogy to the numerical study investigating the impact of rounded edges in the E-plane as described in our previous report, we performed another 2D FE-based numerical study investigating mutual coupling between radiating openings with rounded (aka, filleted) edges. This study investigated the dependence of mutual coupling upon channel separations, choice of fillet radius at the channel openings, and frequency. Figure 2 and Figure 3 summarize the setup of the 2D model. Intermediate boundaries to gently scale the mesh and a perfectly matched layer (PML) outer boundary were incorporated to improve speed and accuracy, respectively. One hundred geometries were considered at 33 frequency values, for a total of 3,300 runs. A plot showing all 3,330 "raw" values of the computed magnitude of S_{21} is provided in Figure 4, while projections of these values against some parameters of interest are shown in Figure 5. The closest to a "single-parameter" dependence of S_{21}(dB) is seen for the channel separation/wavelength.

[1] E.g., see Oliner, A.A. and R.G. Malech, "Radiating Elements and Mutual Coupling," "Mutual Coupling in Infinite Scanning Arrays," and "Mutual Coupling in Finite Scanning Arrays," -- Chaps. 2, 3, and 4 respectively of *Array Theory and Practice*, Vol. II of *Microwave Scanning Antennas*, Ed. by R.C. Hansen, Peninsula Publishing, Los Altos, CA, 1985.

[2] Nishida, S., "Coupled Leaky Waveguides I: Two Parallel Slits in a Plane," *IRE Trans. Ant. and Propagat.*, May, 1960, pp. 323-330. See also Nishida, S., "Coupled Leaky Waveguides II: Two Parallel Slits in a Cylinder," *IRE Trans. Ant. and Propagat.*, July, 1960, pp. 354-360.

Parameter	Range	# of cases
Chan. width:	Fixed at 5.0 cm	1
R_{fil}:	From 1.0 to 10.0 cm, in 1.0 cm steps	10 } → 100 geometries
Gap:	From 1.0 to 10.0 cm, in 1.0 cm steps	10 }
Frequency:	50 to 200 MHz in 25 MHz steps, *plus*	33
	250 to 1500 MHz in 50 MHz steps	→ 3,300 2D-model runs

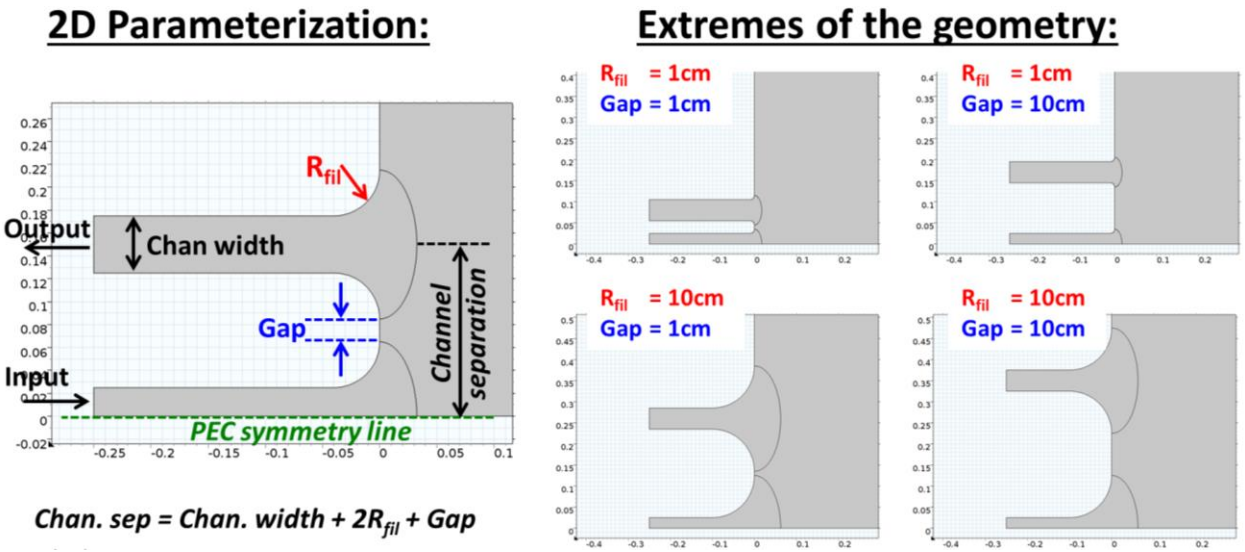

Figure 2. Parameter definitions in 2D E-plane TEM-wave mutual-coupling study.

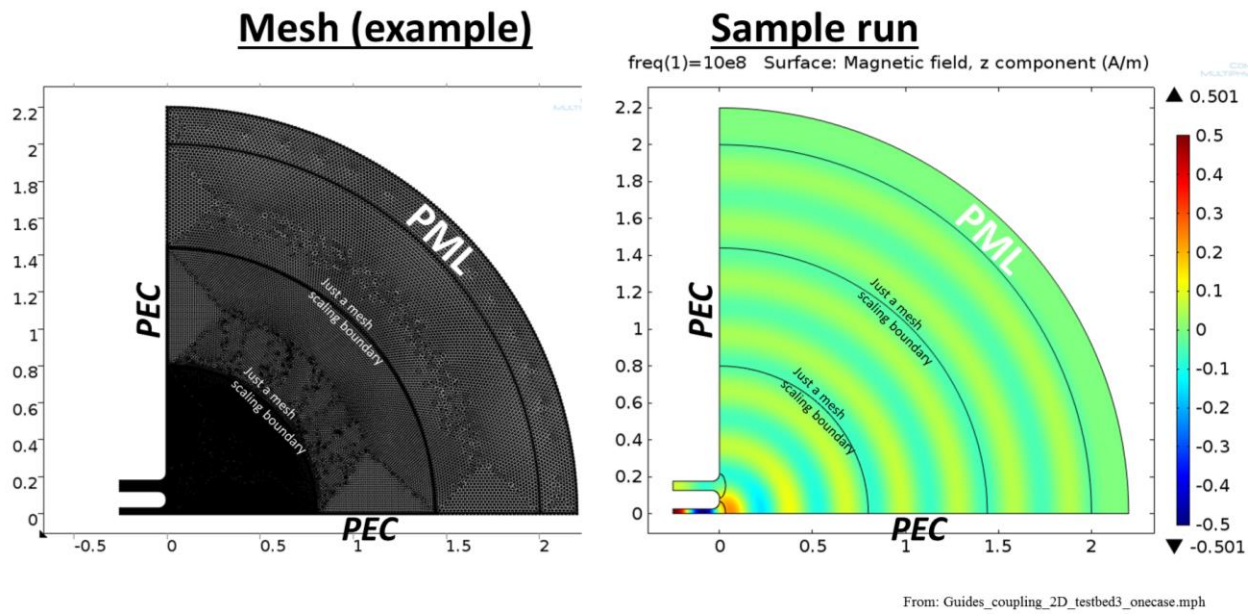

Figure 3. Computation space employed in 2D E-plane TEM-wave mutual-coupling study.

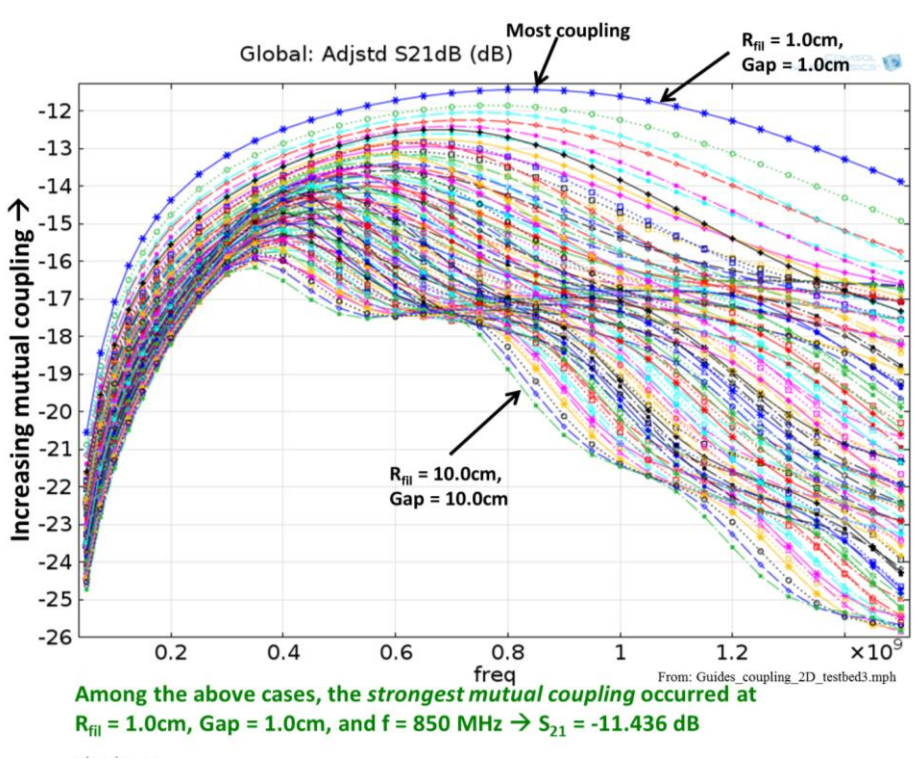

- As expected, strongest mutual coupling occurs when the channels are closest together; weakest coupling when they are farthest apart.
- Coupling becomes *weak at very low frequencies* due to the unavoidably poor impedance match of each channel to its own aperture.
- Coupling also *weakens at sufficiently high frequencies* due to greater *effective* channel separation, rel. to λ.
- Ripples in coupling curves vs. freq are seen in the vicinity of channel separations ~ nλ/2.

Figure 4. Computed S_{21} (dB) vs. frequency (all 3,300 cases)

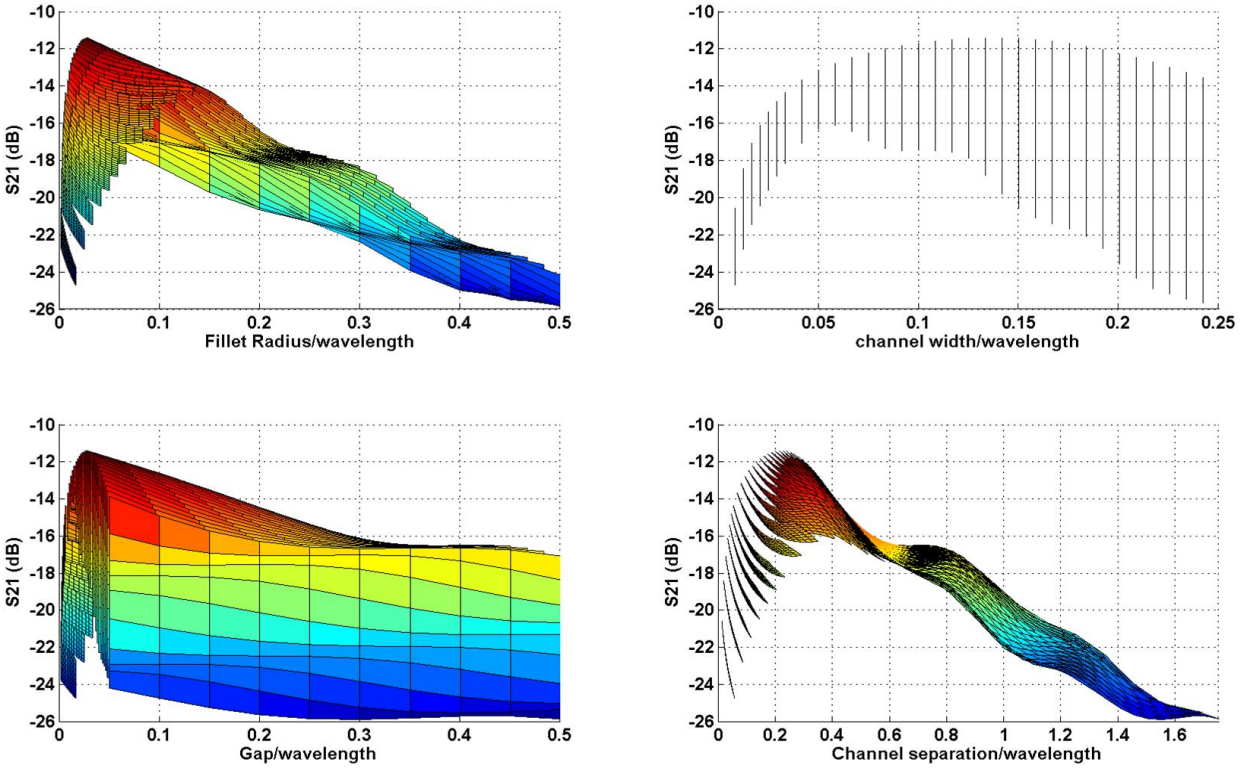

Figure 5. Projections of values in Figure 4 vs. various parameters scaled by wavelength.

Application to 3D

To better understand the implications of the 2D model in a 3D context, we pursued the *following approach* with the help of 3D models:

- Based on the 2D analyses, consider a 3D FAWSEA design likely to exhibit strong mutual coupling, so that any problematic effects of mutual coupling will be easy to observe.
- In particular, noting the highest value of S_{21}(dB) in Figure 4, consider a FAWSEA with f_{TEM} = 850 MHz, with R_{fil} = 1.0cm, Gap = 1.0cm, and channel width = 5cm (yields channel spacing = 8cm).
- Choose the frequency in the 3D model to account for the tilted-wave incidence (vs. normal incidence in the 2D TEM model). I.e., $\lambda_{adj} = \lambda' \cos(\phi_{in})$, where λ' comes from the 2D-model's f_{TEM}=850 MHz. If we choose $\phi_{in} = 30^o$ (a typical value, as noted previously), we obtain f_{3D} = 981.5 MHz.
- Apply the 3D FAWSEA design algorithms & scripts from our previous work, but without a dielectric window (for simplicity), to set the diameters of the grill wires.
- Compare single-channel vs. three-channel 3D configurations, the latter variously with:
  (a) all three channels driven,
  (b) only a single side-channel driven, and
  (c) only the center channel driven.

We selected the following as 3D FAWSEA design parameters (i.e., the *inputs* to our FAWSEA design tools/scripts[3]) : $f_{operating}$ = 981.5 MHz, $\phi_{in} = 30^o$, chan. length = 2.0 m, chan. width = 5.0 cm, R_{fil} = 1 cm, Gap = 1 cm (→ chan. separation = 8 cm), and a constant grill-wire spacing = 6cm. Figure 6 shows the computed wire diameters:

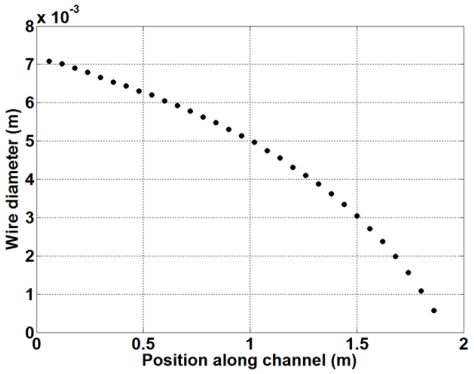

*Applied routines: *fawsea_script_3D0_radiused.m* with *myRpowF.m*

Position	Diameter	Position	Diameter (cont.)
0.06	0.00708204	0.96	0.00513925
0.12	0.00701018	1.02	0.00496521
0.18	0.00690004	1.08	0.00475043
0.24	0.00679323	1.14	0.00455415
0.3	0.0066613	1.2	0.00431537
0.36	0.00654014	1.26	0.00410282
0.42	0.00643618	1.32	0.00387251
0.48	0.00630619	1.38	0.00361951
0.54	0.00620094	1.44	0.00334765
0.6	0.00604983	1.5	0.00303933
0.66	0.00591977	1.56	0.0027051
0.72	0.00577664	1.62	0.00237408
0.78	0.00562465	1.68	0.00198597
0.84	0.00547871	1.74	0.00156414
0.9	0.00530538	1.8	0.00108827
		1.86	0.000577093

With channel depth (initial) = 0.17634777 m.
(Reduced by 2.25% later, to yield clean 30° beam tilt.)

Figure 6. Computed wire diameters vs position for the 3D FAWSEA (with no window) selected for initial use in our mutual-coupling study.

Figure 7 shows a 3D model of a single-channel version of this antenna, including an absorbing termination[4]. Adding two closely-adjacent channels yields the model/results shown in Figure 8. If there was no interaction between the channels, we would expect the gain to increase by $10*\log_{10}(3) = 4.77$dB. But instead, we find the gain has increased by only 3.23dB, the H-plane peak direction has shifted to 28.8^o instead of 30^o, and a slightly smaller fraction of the source power is actually being radiated. Thus, mutual coupling in this example has had a deleterious effect.

[3] Applied scripts/functions: *fawsea_script_3D0_radiused.m* with *myRpowF.m*

[4] In practical designs, the termination would be a conductor, but an absorbing termination allows us to better separate mutual coupling effects from effects due to reflections of non-radiated waves reaching the terminations.

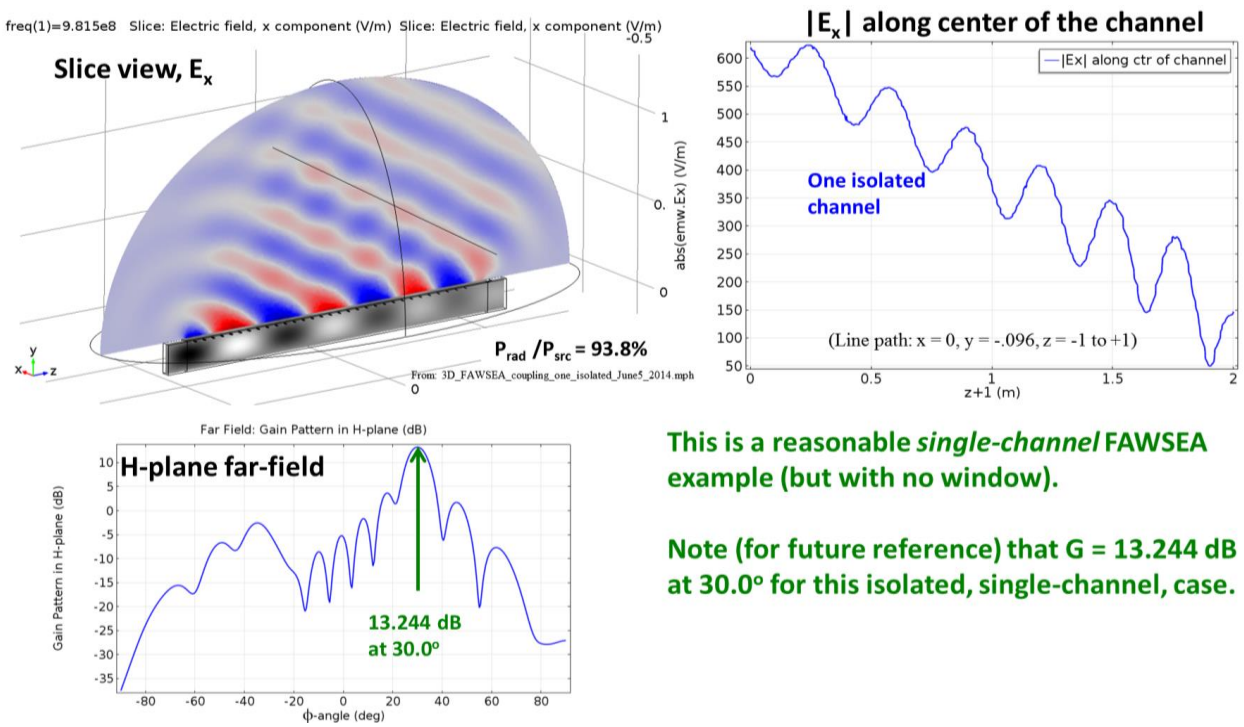

Figure 7. Case of one isolated 3D FAWSEA channel (opening onto a conducting plane).

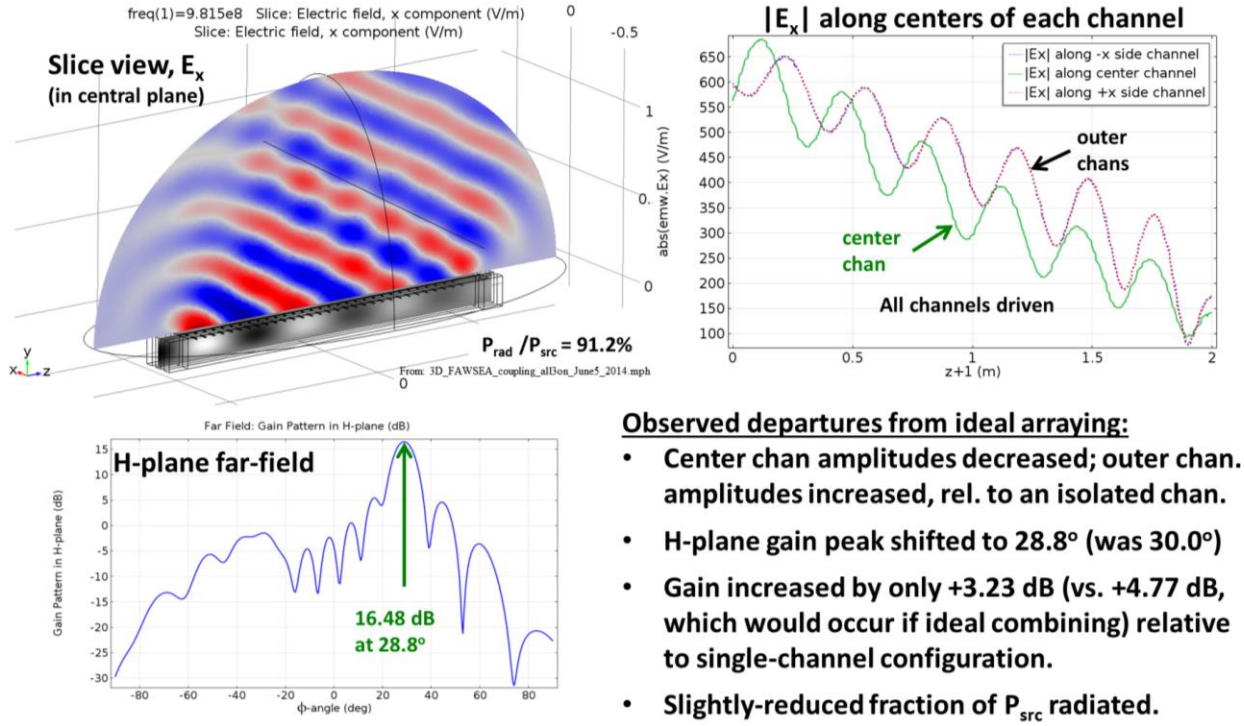

Figure 8. Three tightly-spaced channels, all driven. (Channel spacing = 8 cm)

One perspective by which we can partially understand the reduction in gain is as follows: First, recall that the single isolated channel exhibited gain = 13.244 dB (G_N = 21.106). If we associate this with an effective area, we obtain $A_{eff} = G_N \lambda^2 / 4\pi$ = 15.67 cm^2. Since the channel is 2m long, this implies an effective width W_{eff} = 7.835 cm. However, that ignores the efficiency factor associated with the beam tilt angle. And if we include that term, the effective *length* is reduced to 2m*cos(30^o) and the effective width is *increased* to W_{eff} = 9.047 cm. This width is *larger* than the spacing between the channels in the model of Figure 8. So it makes sense that this three-channel configuration is just too closely-packed, i.e., there is insufficient aperture area available (at least, for the middle channel) to deliver the full array gain. Further understanding follows from the models in Figure 9 and Figure 10, which explore the behavior when only a side-channel is driven and when only the center-channel is driven, respectively. From Figure 9, we see that the presence of the two other channels has a moderate impact on the performance of the driven side-channel (e.g., the gain falls to 12.86 dB). But if just the center channel is driven (Figure 10), the channels immediately on either side impact it severely, with the gain falling to 9.04 dB.

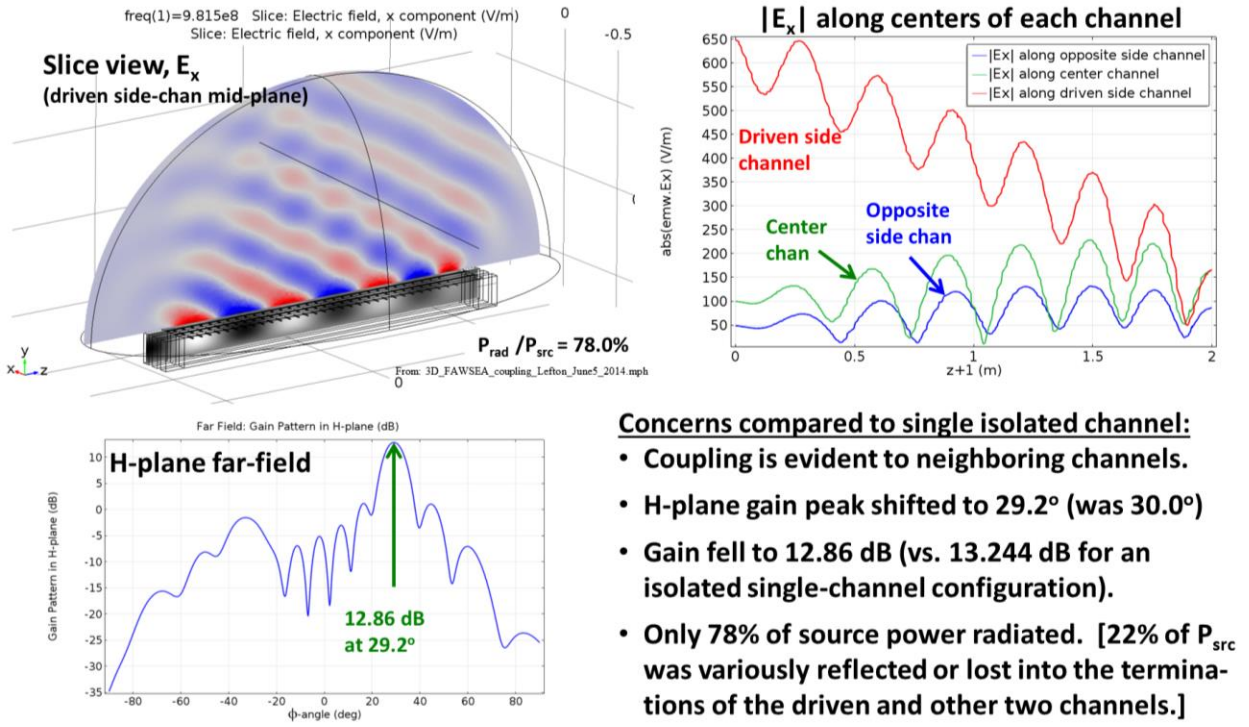

Figure 9. Three tightly-spaced channels, one side-channel driven. Chan. spacing: 8 cm.

To help clarify what to do, Figure 11 revisits some of the curves from Figure 4, highlighting a few of the R_{fil} = 1.0 cm cases with different gaps. Increasing the gap from 1cm to 3cm (which means the channel separation increases from 8cm to 10cm) should reduce the mutual coupling by ~1dB. Is that enough? No. Figure 12 repeats the calculation in Figure 10, but for this modestly-increased spacing. A collapse in gain for the center channel is still there, albeit less dramatic. Clearly, the channels are still too close together. Figure 13 shows the same calculation for a channel-to-channel array spacing of 12cm and Figure 14 shows it for a 14cm spacing. This last case might actually seems pretty good at first look, since the gain of the center channel is very nearly that of the isolated channel case. But a 14cm spacing is well in excess of the "effective width" mentioned earlier, a fact which would *seem* to suggest that the array of three channels, if all operated together, would not produce an appealingly aperture-efficient configuration. But that hypothesis is mistaken, as shown in the model in Figure 15. The gain rises to 18.72 dB! Recall that

the *non-interacting* combination of three 100%-isolated channels of this type should have increased to 13.244 dB + $10\log_{10}(3)$ = 18.015 dB. So. where did the *extra* +0.7 dB come from? {continues, page 14}

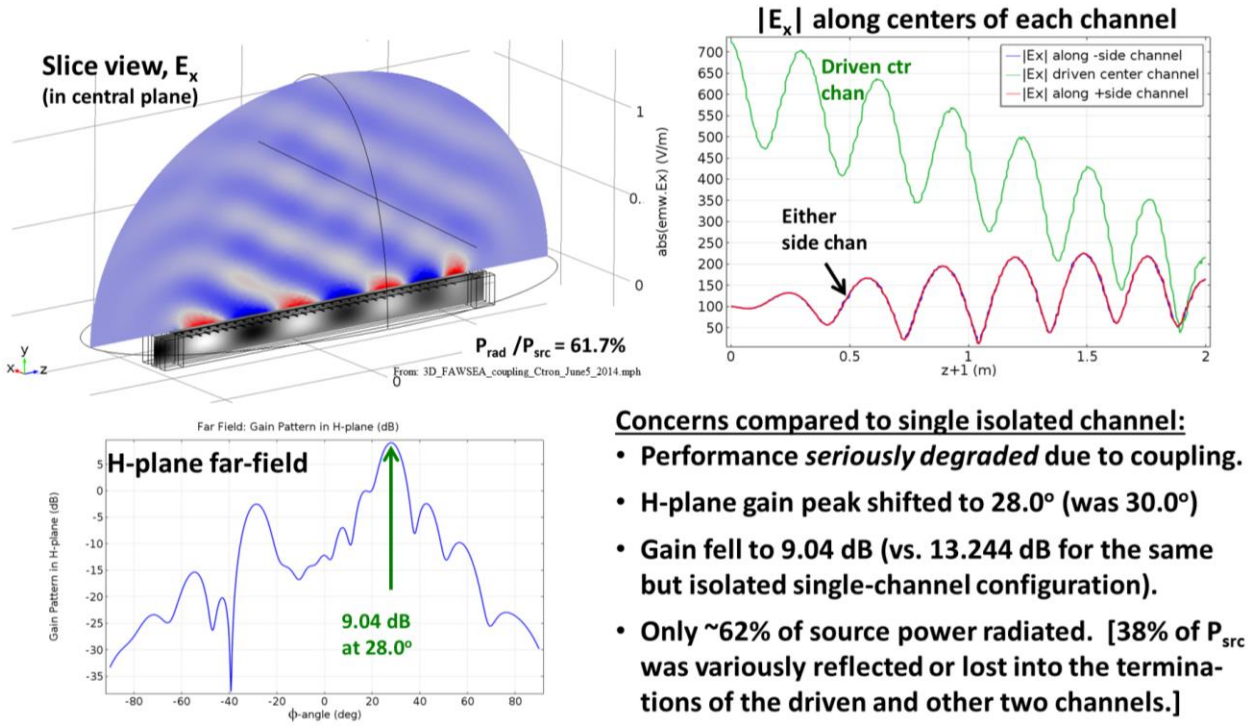

Figure 10. Three tightly-spaced channels, center-channel driven. Chan. spacing: 8 cm.

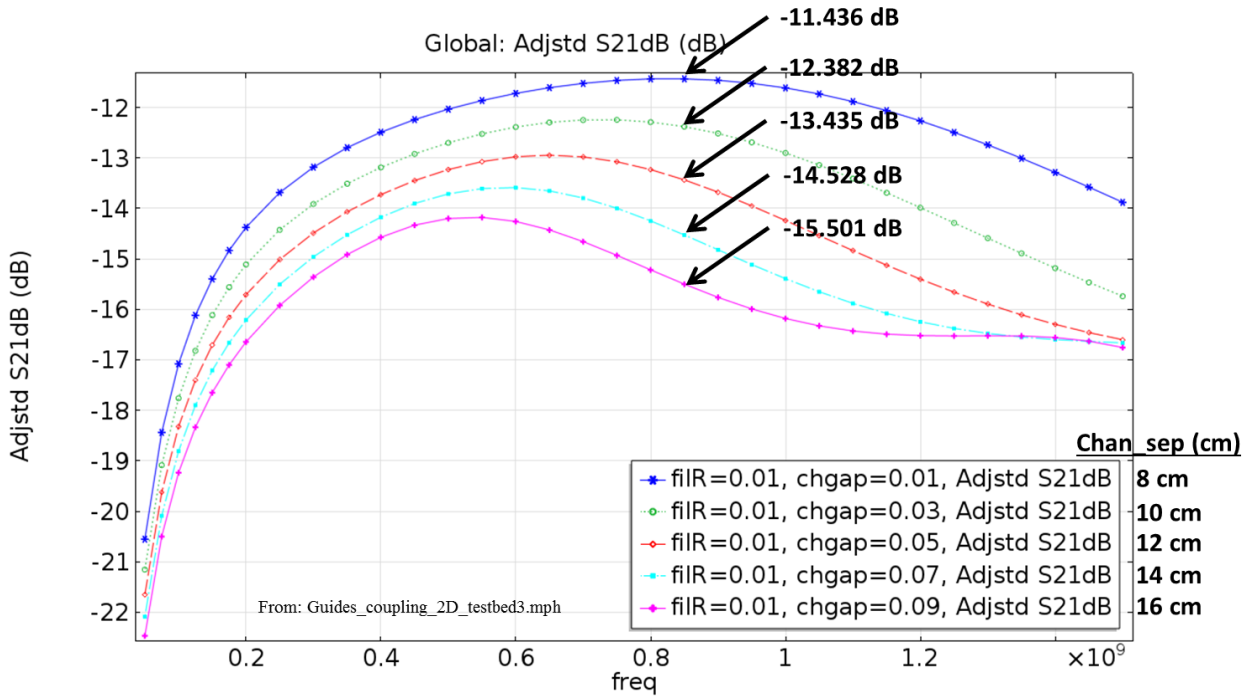

Figure 11. Selected curves from Figure 4, showing falling S_{21} as channel separation rises.

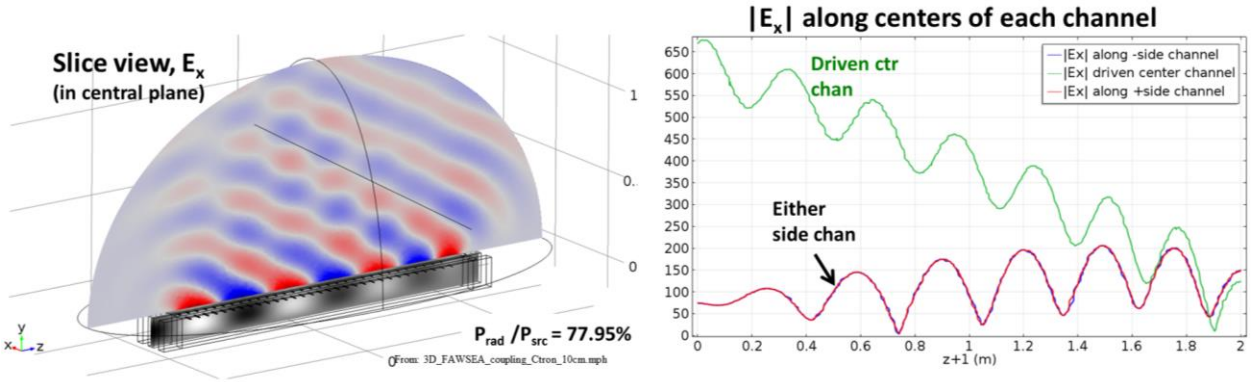

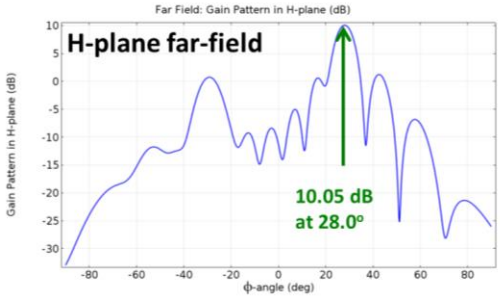

Compared to center-channel driven at 8cm spacing:

- **Performance *improved* due to less coupling**
- **H-plane gain peak still at ~ 28.0° (instead of 30°)**
- **Gain is 10.05 dB (vs. 9.04dB dB for 8cm channel spacing) but was 13.244dB for isolated chan.**
- **~78% of P_{src} radiated. (vs ~62% for 8cm channel spacing) but was 93.8% for isolated chan.**

Figure 12. Three channels, with only center-channel driven. Chan. spacing = 10 cm.

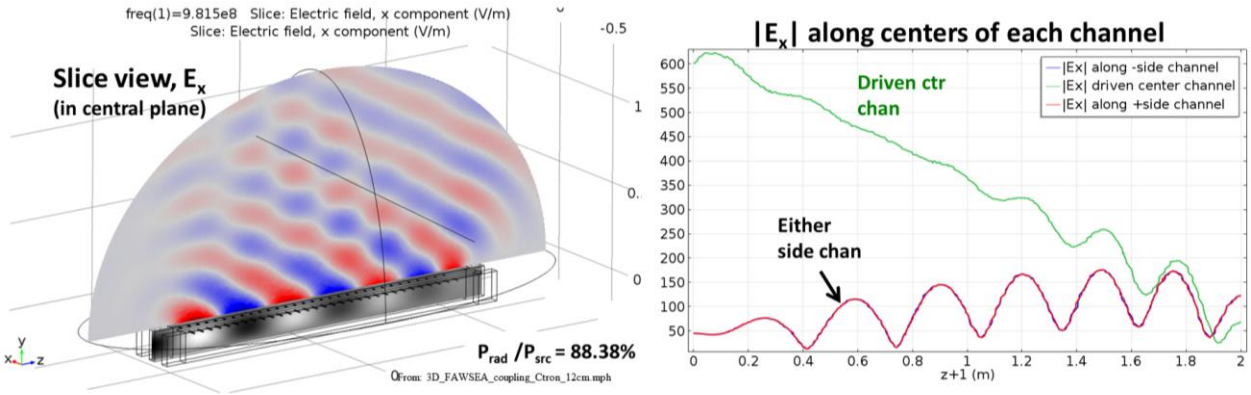

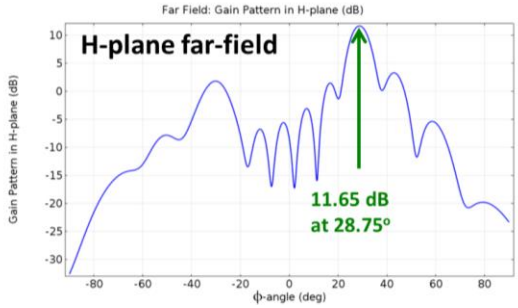

Compared to center-channel driven at 8cm spacing:

- **Performance *improved* due to less coupling**
- **H-plane gain peak is at ~28.75° (instead of 30°)**
- **Gain is 11.65 dB (vs. 9.04dB dB for 8cm channel spacing) but was 13.244dB for isolated chan.**
- **~88% of P_{src} radiated. (vs ~62% for 8cm channel spacing) but was 93.8% for isolated chan.**

Figure 13. Three channels, with only center-channel driven. Chan. spacing = 12 cm.

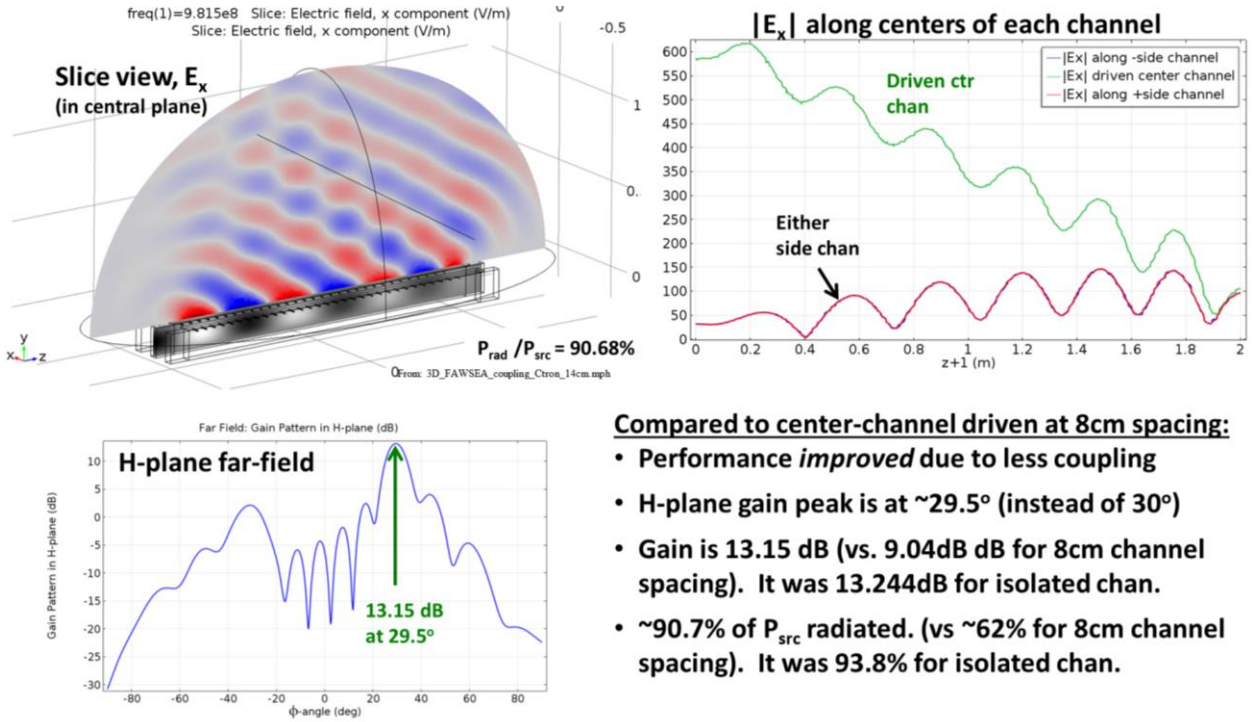

Compared to center-channel driven at 8cm spacing:

- **Performance *improved* due to less coupling**
- **H-plane gain peak is at ~29.5° (instead of 30°)**
- **Gain is 13.15 dB (vs. 9.04dB dB for 8cm channel spacing). It was 13.244dB for isolated chan.**
- **~90.7% of P_{src} radiated. (vs ~62% for 8cm channel spacing). It was 93.8% for isolated chan.**

Figure 14. Three channels, with only center-channel driven. Chan. spacing = 14 cm.

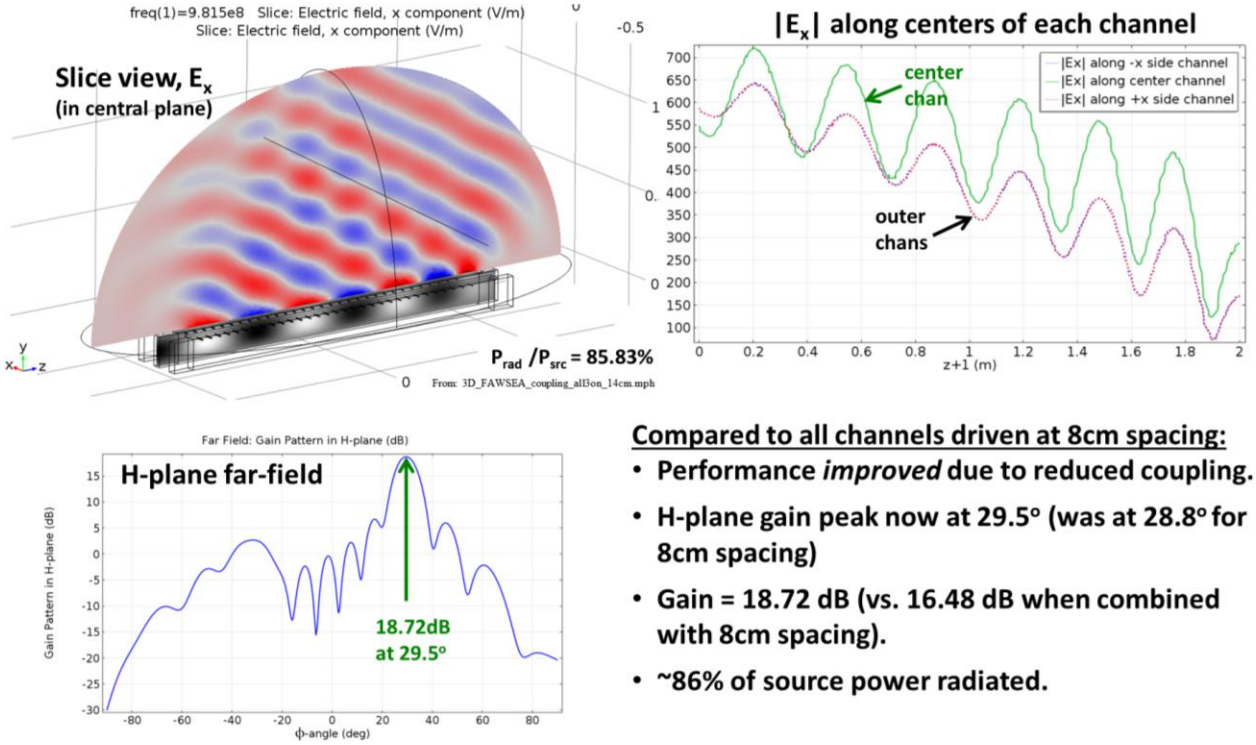

Compared to all channels driven at 8cm spacing:

- **Performance *improved* due to reduced coupling.**
- **H-plane gain peak now at 29.5° (was at 28.8° for 8cm spacing)**
- **Gain = 18.72 dB (vs. 16.48 dB when combined with 8cm spacing).**
- **~86% of source power radiated.**

Figure 15. Three channels, all driven. Channel spacing = 14 cm.

The answer is that as we increased the channel-to-channel spacing (and as we observed the center channel gain increasing) the gains associated with the side channels were actually increasing faster, and actually *exceeded* that of the isolated-channel case. In other words, the mutual coupling of each *side channel* to the other two channels *enhanced* the gain. Though initially surprising, this behavior is hardly without precedent in antenna-arrays; it is due to constructive interference from parasitic channels – analogous to the sort of behavior used to advantage in Yagi-Uda antennas, for example. Figure 16 reveals this effect further by modeling the case where the spacing is once again 14cm, but only one side-channel is driven. The gain of this side channel (in interaction with the two parasitic channels off to one side) is 14.4dB, which is about 1.16dB *more* than that from a single channel alone.

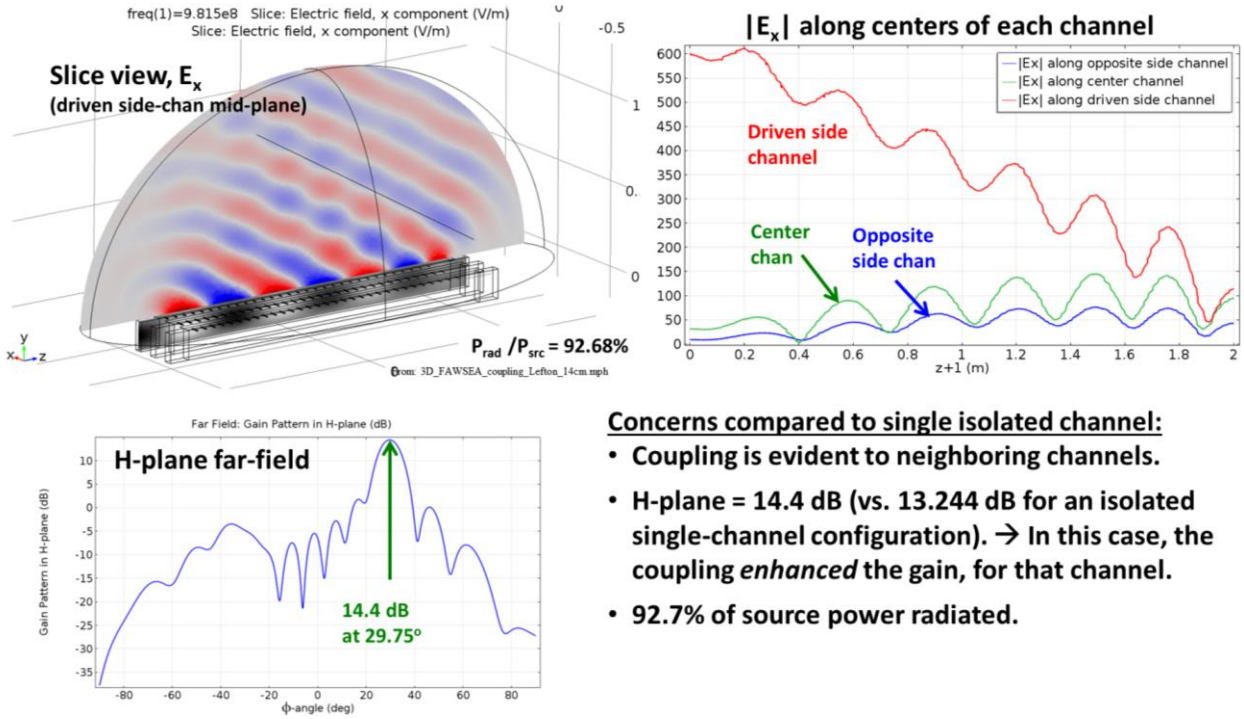

Figure 16. Three channels, only one side channel driven. Channel spacing = 14 cm.

Now, despite the arguably-unexpected 18.72 dB gain computed (per Figure 15) for the all three channels-driven design with 14cm spacing, this design is still somewhat problematic. The *total* aperture width (if we associate +4.5cm extensions on each side, per W_{eff} noted earlier) is ~28+9 = 37cm, yielding a physical aperture area ~0.74m^2. The aperture efficiency corresponding to this 18.72 dB gain at 981.5 MHz for that much area follows immediately, as 74.7%. That's respectable, although we have done somewhat better in other FAWSEA designs. We are more concerned about the imbalanced aperture field distribution. Figure 17 shows slices of |E| at 2, 4, and 6 cm from the aperture. The magnitude of the field is more non-uniform spatially than desirable, a condition which could encourage surface breakdown.

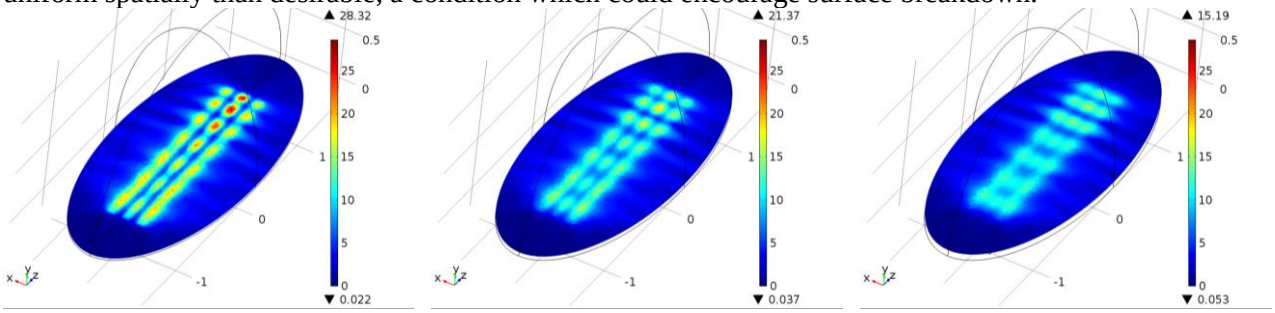

+2cm from aperture **+4cm from aperture** **+6 cm from aperture**

Figure 17. |E| (kV/cm) in vicinity of the aperture for the Figure 15 design, if P_{src} ~1 GW.

Generally, it is desirable to ensure more-uniform aperture surface fields and to reduce the imbalance in the behavior of interior vs exterior channels. For example, consider a design like the one in Figure 15, but with R_{fil} increased to 4cm and the gap reduced to 1cm, again yielding 14cm for the channel-to-channel separation. (Strictly speaking, we should now re-compute the grill wire diameters, but let's just keep them unchanged for now.) Figure 18 shows the predicted performance after this change, which also happens to deliver 0.5 dB more gain than the arrangement in Figure 15.

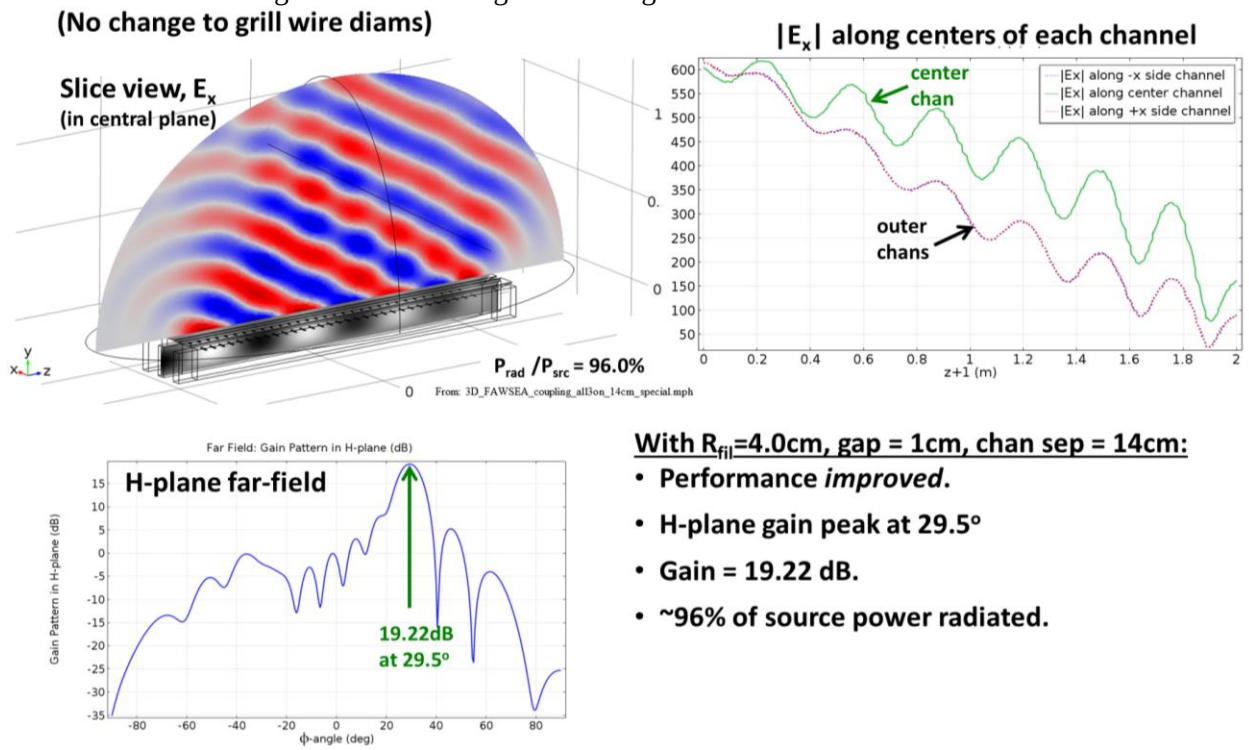

Figure 18. Three channels, all driven, R_{fil} increased to 4cm. Channel spacing = 14 cm.

Also, Figure 19 shows a smoother distribution of |E| near the aperture than that appearing in Figure 17.

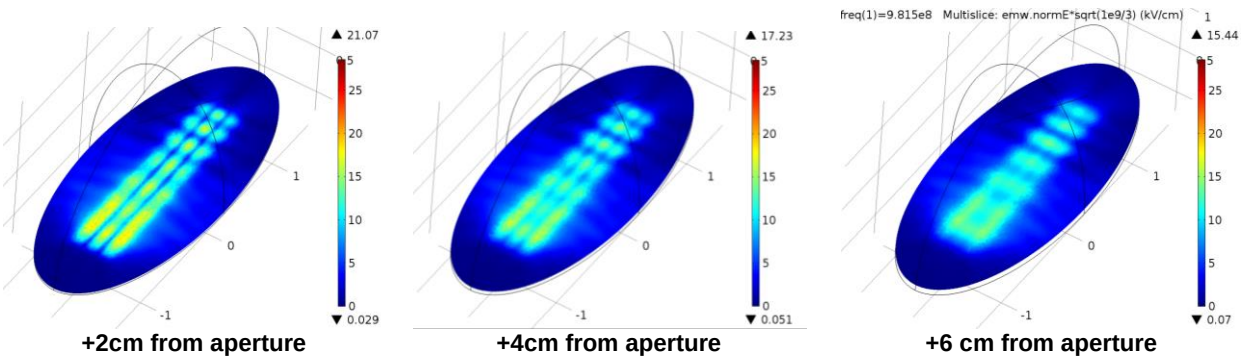

Figure 19. |E| (kV/cm) in vicinity of the aperture for the Figure 18 design, if P_{src} ~1 GW.

We will continue the discussion of mutual coupling and the challenges and opportunities it represents in regard to the optimization of aperture field distributions in our next report.

3.2. Compensating for Modified Phase-velocities in Leaky-wave Channels

Our earlier analyses (described in our earlier reports) set-aside the question of explicitly computing the phase velocity of the wave in a leaky-guide, which differs somewhat from that in a closed-wall guide. For only slight leakage the difference is small, but it becomes more pronounced if the grill is leakier. For theoretical completeness and to speed-up the design process, the necessary adjustment[5] is described here.

Recall that for a *uniform* grill and wave incident at angle θ relative to normal, we previously noted that the *complex reflection coefficient* at the grill was given by:

$$R_g = \frac{-\left(X_a - X_b\right)^2 - Z_0^2 + X_a^2}{\left(Z_0 + j\left(X_a - X_b\right)\right)^2 + X_a^2},$$

where expressions for X_a and X_b are given by Marcuvitz (1951) and (for his expressions) Z_0 can be normalized to unity. In fact, computation of R_g was *already included* in our previously-documented custom MatLab functions. The next step to computing the detailed impact upon the phase velocity within the leaky guide is to recognize that, *in this context*, the grill behaves very much as if it were equivalent to a perfectly-conducting wall moved slightly farther out from the opposite side wall of the waveguide. (See Figure 20 for the basic idea.) Thus, in practice, all we need to do is compute the value of δ_{xtra} . Once we have that, we'll know where to place our grill wires to match the phase velocity in the feeding waveguide. It is clear that the distance δ_{xtra} corresponds to an equivalent phase factor = exp(2j*k_0*δ_{xtra}/cosθ). But since the reflection coefficient at a PEC wall is *real*, the *imaginary* part of R_g (if its magnitude is normalized) must come *solely* from this term. Thus:

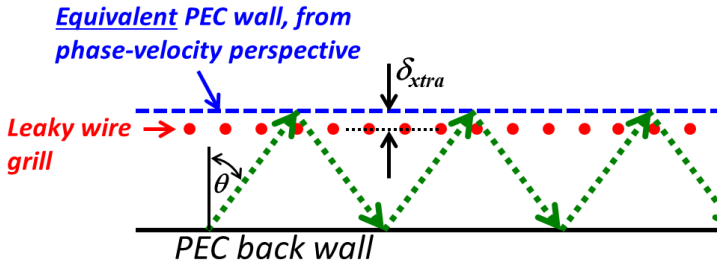

Figure 20. Concept of a *virtual* perfectly-conducting wall for the phase-velocity computation. (Note: this is an H-plane view; E is normal to the page)

$$\frac{imag\left(R_g\right)}{\left|R_g\right|} = \sin\left(2k_0\delta_{xtra}/\cos\theta\right), \text{ which immediately yields: } \boxed{\delta_{xtra} = \frac{\cos\theta}{2k_0}\sin^{-1}\left[\frac{imag\left(R_g\right)}{\left|R_g\right|}\right]}$$

Of course, since R_g varies as a function of position if we change the diameters (or spacing) of the wires as a function of position, then any generalized δ_{xtra} will also vary as a function of position, suggesting (as we have previously-noted) correction methods such as tilting the back-wall and/or otherwise shifting the grill wire positions relative to the back-wall to hold the phase velocity ~constant throughout the channel. For future reference, a custom MatLab function to compute δ_{xtra} via the above rule is provided in Figure 21.

```
% function DeltaXtra = DeltaXtra(AngIn,a,d,freq)
% AngIn = angle of inc. rel to normal, in radians
% a = wire spacing in meters
% d = wire diameter in meters
% freq = frequency in Hz
% Computes distance from grill to equiv PEC wall.
% Used for FAWSEA design.  E is parallel to wires.
% Prepared by R. Koslover, SARA, Inc.
% June, 2014
% See Marcuvitz, Waveguide Handbook, p.286.
% See also Quarterly Report #3, SARA Proj: Navy41.
function DeltaXtra = DeltaXtra(AngIn,a,d,freq)
    ct = cos(AngIn);
    st = sin(AngIn);
    c_const = 2.99792458e8; %c in m/s
    lambda = c_const/freq; % free space wavelength
sum1 = 0;
sum2 = 0;
for m = 1:1:1000
        sum1 = sum1+1/sqrt(m^2+2*m*a*st/lambda-
(a*ct/lambda)^2)-1/m;
        sum2 = sum2+1/sqrt(m^2-2*m*a*st/lambda-
(a*ct/lambda)^2)-1/m;
    end
   % Normalized to Z0 = 1 everywhere
   % Compute Xa using sum from Marcuvitz, p. 286
    Xa = (a*ct/lambda)*(log(a/(pi*d))+0.5*(sum1+sum2));
    Xb = (a*ct/lambda)*(pi*d/a)^2;
    Zeq = j*(Xa-Xb)-(Xa^2)/(-1+j*(Xb-Xa));
    gam = (Zeq-1)/(Zeq+1);
    DeltaXtra =
(ct*lambda/(4.0*pi))*asin(imag(gam)/abs(gam)); % meters
end
```

Figure 21. Listing of custom MatLab function 'DeltaXtra' that computes δ_{xtra}.

[5] This calculation is only strictly valid in the ideal 2D case (H-plane analyses only) with no dielectric window, but may be generalizable, as will be discussed shortly.

A plot of computed δ_{xtra} vs wire diameters at selected wire spacings is provided in Figure 22.

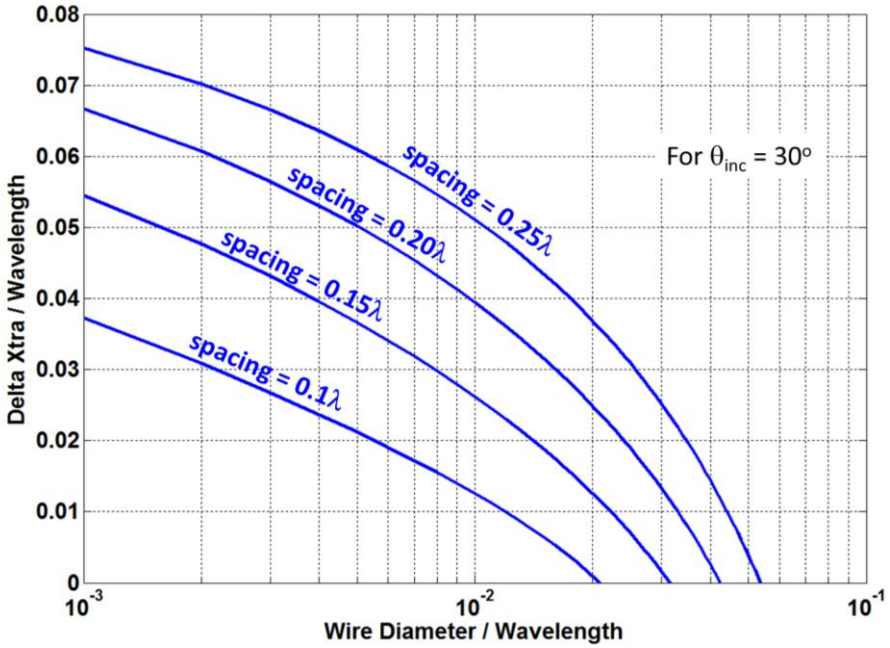

Figure 22. Computed δ_{xtra} vs wire diameter for various wire spacings, scaled to the free-space λ, for $\theta_{inc}=30^o$.

Although we have derived δ_{xtra} from the imaginary component of the wire-grill reflection coefficient R_g, *this could be generalized, in principle,* to use the imaginary component of the *overall* reflection coefficient, the latter found via the wave-matrix formalism (see previous reports), thus effectively accounting for curved channel edges in the E-plane, a dielectric window, and even other[6] factors when positioning the wire grill. However, it is unclear if additional adjustments to the grill or opposite wall that would follow from doing those more-complete calculations would prove significant. We may revisit this later.

3.3. Aperture Options for Forward-traveling Leaky-wave HPM Antennas

The far-field gain of any aperture-type antenna has an upper-bound which is generally only realizable with an ideal distribution of aperture illumination. For flat apertures, the most ideal illumination is 100% uniform[7] in terms of magnitude, polarization, and phase. Traveling-wave leaky-wave antennas cannot deliver uniform phase, but they can deliver fairly-uniform magnitude and polarization, with nearly-linear phase along the aperture. The latter results in a non-zero tilt angle of the beam relative to the aperture normal. Considered separately from other factors, this imposes a factor of $\cos(\phi_{tilt})$ on the numerical gain, where ϕ_{tilt} is the beam tilt angle. This reduces the effective area: $A_{leaky} = A_{geo}\cos\phi_{tilt}$. Source bandwidths, cutoff considerations, and finite-duration pulse considerations typically lead us to choose $\phi_{tilt} > \sim 20^o$ or so for practical HPM-capable designs. In particular, selecting ϕ_{tilt} ~25-35^o often provides a satisfying tradeoff between bandwidth and gain. Note that within that range, the tilt-related efficiency-factor ranges from $\cos(25^o) = 90.6\%$ to $\cos(35^o) = 81.9\%$. However, there is more to describing antenna patterns than noting the peak gains achievable, and there are many more apertures of interest than those that are simple and flat.

[6] For example, one could potentially account for the curved section between the grill and aperture in a RAWSEA.
[7] We exclude "super-gain" class antennas, as their extremely high-Q configurations preclude HPM/DEW applications and, in fact, most other applications as well. Note also that the far-fields of non-aperture (e.g., wire-type) antennas can also be characterized by the approach to be described here, but it is generally less useful to do so than to employ alternative methods integrating over their surface currents.

We are currently cataloging some of the aperture shapes we consider to be of most interest, along with associated antenna patterns and their anticipated practically-achievable aperture efficiencies. Of course, curved apertures are usually less aperture efficient than flat ones, but may still deliver quite-respectable and operationally-practical gain, especially when compensating feed schemes are introduced (such as we have noted in earlier analyses). For reference, several of the aperture geometries in our current study are shown in Figure 23, along with example representative aperture fields, although the latter (in these particular examples) are shown without distributed phase delays or other compensation for gain-sapping aperture curvature. Note also that the sizes and aspect ratios of the apertures shown here were chosen arbitrarily, i.e., they are not intended to represent any particular candidate HPM DEW platforms.

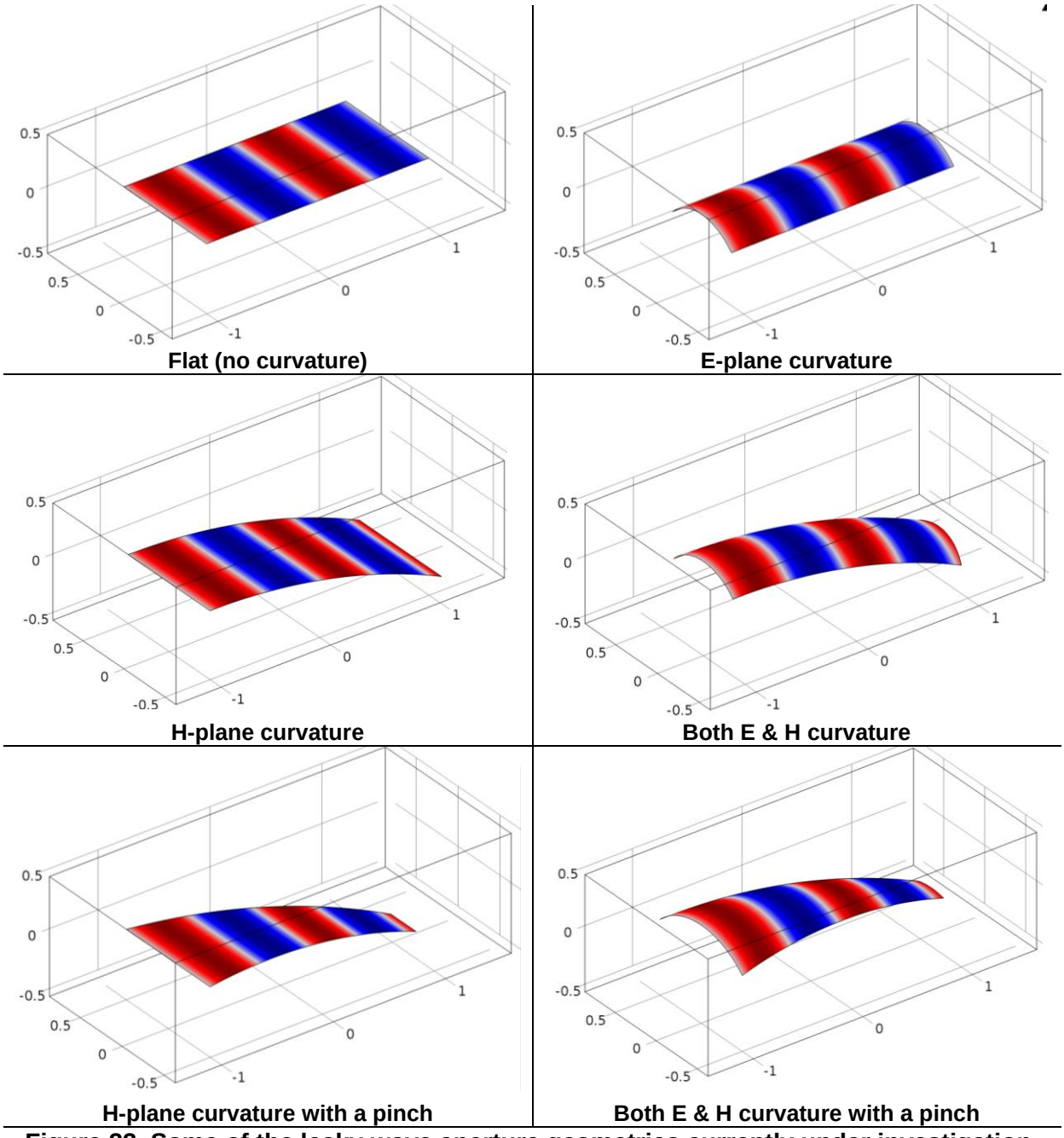

Figure 23. Some of the leaky-wave aperture geometries currently under investigation. (Note: Only the *apertures* are highlighted above, for simplicity.)

We are exploring the far-field patterns that can be generated by forward-traveling, leaky-wave field distributions in apertures that are variously flat, curved in the E-plane, curved in the H-plane, curved in both planes, or curved and/or pinched more creatively. Field re-distribution schemes to compensate, at least in part, for the gain-degrading effects of aperture curvatures are also being studied. For future reference, we note that for computation of the far-fields from all these antennas, we are currently using the following balanced aperture-integration approximation formula[8], which is among the more practical/useful[9] expressions available:

$$\vec{E}_p = \frac{jk}{4\pi}\hat{r}_p \times \iint_s \left[\hat{n}\times\vec{E}_a - \eta\hat{r}_p \times \left(\hat{n}\times\vec{H}_a\right)\right]\exp\left(jk\vec{r}_a\cdot\hat{r}_p\right)dS$$

where $\vec{E}_p$ is the computed electric field at the far-field point *p*, $\vec{E}_a$ and $\vec{H}_a$ are the electric and magnetic complex vector fields on the aperture (or surface *S* enclosing the antenna), $\hat{n}$ is the unit outward normal on the aperture (or surface *S*), η is the impedance of free space (~377 Ohms), k is the free space wave number ($2\pi/\lambda$), $\vec{r}_a$ is the vector from the origin to the aperture field point, $\vec{r}_p$ is the vector from the origin to the radiated field point, with $\hat{r}_p = \vec{r}_p \big/ \left|\vec{r}_p\right|$ = a unit vector along $\vec{r}_p$. In cartesian coordinates, $\hat{r}_p = \hat{x}\sin\theta_p\cos\phi_p + \hat{y}\sin\theta_p\sin\phi_p + \hat{z}\cos\theta_p$. [Note: for a uniform-field flat aperture in the *xy*-plane, the above surface integral simplifies greatly and it is fairly easy to show that the resulting expression for E_p at θ_p =0 is consistent with on-axis gain $G_{ideal} = 4\pi A_{geo}\big/\lambda^2$.] Of course, analytic or semi-analytic expressions for E-plane and H-plane cuts of far-field patterns for a variety of idealized aperture antenna distributions can be found in the literature[10], although most are limited to planar apertures, especially those with rectangular or circular boundaries. (Recall also the previously-noted the works of Honey, Ishimaru, and others in analyzing leaky-wave antennas and apertures conformal to ideal flat or cylindrical surfaces.) For greater generality, our approach here is, and will continue to be, mostly numerical. We have previously implemented the aforementioned aperture-field integration expression for E_p in a variety of circumstances and in some cases have used more complicated forms to compute radiating near-fields and time-domain responses, although those are not expected to be needed here.

In our next report, we plan to include a summary of the flat and curved aperture shapes studied, more information about the leaky-waveguide structures that are so essential to fitting these apertures and enabling their practical realization, and their predicted/anticipated performance characteristics of these novel antennas, including (but not limited to) their predicted far-field patterns.

4. DISCUSSION, CONCLUSIONS, AND RECOMMENDATIONS

We are pleased to report that the work performed during this 3rd quarter of the R&D program has continued to advance this important technology and to extend the tool set available to would-be designers of leaky-wave based HPM antennas. We look forward to both extending the theory and developing and documenting in our next report a set of representative example designs to better guide the engineering of these antennas. We appreciate ONR's continued support for this R&D.

---

[8] S. Silver, *Microwave Antenna Theory and Design.* See especially Sec. 5-11, "The Aperture Field Method," and Sec. 5-12, "The Fraunhofer Region." From 1st Ed, publ. by office of Scientific Research and Development, National Defense Research Committee, NY, 1949. See http://www.jlab.org/ir/MITSeries/V12.PDF .

[9] This particular expression is especially convenient numerically, since it contains no derivatives.

[10] See, among others, Jull, E.V., "Radiation from Apertures," Chap. 5 of *Antenna Handbook: Theory, Applications, and Design,* Ed. by Y.T. Lo and S.W. Lee, Van Nostrand Reinhold, NY, 1988.

BIBLIOGRAPHY (alphabetical)

Goldstone, L.O. and Oliner, A.A., "Leaky-Wave Antennas I: Rectangular Waveguides," *IRE Trans. Ant. and Propagat*., Oct., 1959, pp. 307-319.

Goldstone, L.O. and Oliner, A.A., "Leaky-Wave Antennas II: Circular Waveguides," *IRE Trans. Ant. and Propagat*., May., 1961, pp. 280-290.

Honey, R.C., "A Flush-Mounted Leaky-Wave Antenna with Predictable Patterns," *IRE Trans. Antennas and Propagat*., 7, pp. 320-329, 1959.

Ishimaru, A.K. and Beich, F.R., "Pattern Synthesis With a Flush-Mounted LeakyWave Antenna on a Conducting Circular Cylinder," *J. of Res. of the Nat. Bureau of Standards-D. Radio Propagat* Vol. 66D, No.6, Nov- Dec. 1962, pp. 783-796.

Jull, E.V., "Radiation from Apertures," Chap. 5 of *Antenna Handbook: Theory, Applications, and Design*, Ed. by Y.T. Lo and S.W. Lee, Van Nostrand Reinhold, NY, 1988.

Marcuvitz, N., *Waveguide Handbook*, McGraw-Hill, NY, 1951.

Nishida, S., "Coupled Leaky Waveguides I: Two Parallel Slits in a Plane" *IRE Trans. Ant. and Propagat*., May, 1960, pp. 323-330.

Nishida, S., "Coupled Leaky Waveguides II: Two Parallel Slits in a Cylinder," *IRE Trans. Ant. and Propagat.*, July, 1960, pp. 354-360.

Oliner, A.A. and R.G. Malech, "Radiating Elements and Mutual Coupling," "Mutual Coupling in Infinite Scanning Arrays," and "Mutual Coupling in Finite Scanning Arrays," -- Chaps. 2, 3, and 4 respectively of *Array Theory and Practice*, Vol. II of *Microwave Scanning Antennas*, Ed. by R.C. Hansen, Peninsula Publishing, Los Altos, CA, 1985.

Oliner., A.A, and D.R. Jackson, "Leaky Wave Antennas," Chap. 11 of *Antenna Engineering Handbook*, 4th Ed., Edited by J.L. Volakis, McGraw-Hill, NY, 2007.

Silver, S., *Microwave Antenna Theory and Design*, 1st Ed, publ. by office of Scientific Research and Development, National Defense Research Committee, NY, 1949.

SUGGESTED DISTRIBUTION LIST

Official Record Copy
Mr. Lee Mastroianni
E-Mail: lee.mastroianni@navy.mil
Code 30
Office of Naval Research
875 North Randolph St.
Arlington, VA 22203-1995 1 cy

Dr. Joong H. Kim
E-Mail: joong.kim@navy.mil
Code 30
Office of Naval Research
875 North Randolph St.
Arlington, VA 22203-1995 1 cy

Director, Naval Research Lab
E-mail: reports@library.nrl.navy.mil
Attn: Code 5596
4555 Overlook Avenue, SW
Washington, D.C. 20375-5320 1 cy

Defense Technical Information Center
E-mail: tr@dtic.mil
8725 John J. Kingman Road
STE 0944
Ft. Belvoir, VA 22060-6218 1 cy

Dr. Donald Shiffler
AFRL/RDH
Kirtland AFB, NM 87117-5776 1 cy

Dr. Michael Haworth
AFRL/RDHP
Kirtland AFB, NM 87117-5776 1 cy

Dr. Andrew D. Greenwood
AFRL/RDHE
Kirtland AFB, NM 87117-5776 1 cy

Dr. Susan Heidger
AFRL/RDH
Kirtland AFB, NM 87117-5776 1 cy

Matthew McQuage
Naval Surface Warfare
Dahlgren Division 1 cy

Michael Wagaman
Advanced Technology Directorate
PEO Strike Weapons and Unmanned Aviation
Patuxent River, MD. 1 cy

Dr. Frank E. Peterkin
Director
Directed Energy Technology Office
Dahlgren, VA 1 cy

LTC Chuck Ormsby
Chief
Directed Energy Requirements
Langley AFB, VA 1 cy

Patrick Randeson
Science, Technology and Weapons Analyst
Central Intelligence Agency
Washington, D.C. 1 cy